

See discussions, stats, and author profiles for this publication at: <https://www.researchgate.net/publication/266562735>

A robust global and local mixture distance based non-rigid point set registration(including source codes->link data)

Article in Pattern Recognition · January 2015

DOI: 10.1016/j.patcog.2014.06.017

CITATIONS

89

READS

1,512

3 authors:



Yang Yang

Yunnan Normal University

61 PUBLICATIONS 692 CITATIONS

[SEE PROFILE](#)



Sim Heng Ong

National University of Singapore

275 PUBLICATIONS 5,142 CITATIONS

[SEE PROFILE](#)



Kelvin W. C. Foong

National University of Singapore

113 PUBLICATIONS 1,783 CITATIONS

[SEE PROFILE](#)

Some of the authors of this publication are also working on these related projects:



Project

Environment monitoring and prediction [View project](#)



Project

GIS papers [View project](#)



A robust global and local mixture distance based non-rigid point set registration



Yang Yang ^{a,b,c,d,*}, Sim Heng Ong ^{d,e,f}, Kelvin Weng Chiong Foong ^{d,g}

^a School of Information Science and Technology, Yunnan Normal University, Kunming 650092, Yunnan, China

^b The Engineering Research Center of GIS Technology in Western China of Ministry of Education of China, Yunnan Normal University, Kunming 650092, Yunnan, China

^c Key Laboratory of Education Informatization for Nationalities of Ministry of Education of China, Yunnan Normal University, Kunming 650092, Yunnan, China

^d NUS Graduate School for Integrative Sciences and Engineering, National University of Singapore, Singapore 117456, Singapore

^e Department of Electrical and Computer Engineering, National University of Singapore, Singapore 117576, Singapore

^f Department of Bioengineering, National University of Singapore, Singapore 117576, Singapore

^g Faculty of Dentistry, National University of Singapore, Singapore 119083, Singapore

ARTICLE INFO

Article history:

Received 29 May 2013

Received in revised form

14 April 2014

Accepted 19 June 2014

Available online 28 June 2014

Keywords:

Non-rigid point set registration

Global and local mixture distance

Correspondence estimation

Transformation updating

Multi-feature based framework

ABSTRACT

We present a robust global and local mixture distance (GLMD) based non-rigid point set registration method which consists of an alternating two-step process: correspondence estimation and transformation updating. We first define two distance features for measuring global and local structural differences between two point sets, respectively. The two distances are then combined to form a GLMD based cost matrix which provides a flexible way to estimate correspondences by minimizing global or local structural differences using a linear assignment solution. To improve the correspondence estimation and enhance the interaction between the two steps, an annealing scheme is designed to gradually change the cost minimization from local to global and the thin plate spline transformation from rigid to non-rigid during registration. We test the performance of our method in contour registration, sequence images and real images, and compare with six state-of-the-art methods where our method shows the best alignments in most scenarios.

© 2014 Elsevier Ltd. All rights reserved.

1. Introduction

Non-rigid point registration is the process of aligning one set of points (the source point set) to another (the target point set) that is deformed from the former. It plays a key role in many computer vision, medical imaging and pattern recognition applications, such as generating cartoon animation, object retrieval, recovering dynamic motions of human organs and muscles, and template matching for hand-written characters. According to the methodological differences of current non-rigid point set registration methods, there are two major types of classification: (a) iterative or non-iterative methods, and (b) learning or non-learning based methods. Since we mainly focus on developing an iterative method in this work, we introduce and discuss the current methods amongst the first classification (a).

In non-iterative methods, correspondences between two point sets are recovered under a single estimation using high level

structures such as lines [1], curves [2], surfaces [3], shape context descriptors [4,5] and graph relations [6,7]. Shape context descriptors [4,5] and graphs [6,7] are two of the most popular features for non-iterative methods. The methods [4,5,8–12] based on such features seek to minimize the point distribution or graph relation differences between two point sets for finding correspondences. Recently, learning graph based methods [9,10,12] were introduced and the results show the parameter learning to be vital for improving the matching accuracy. However, the applicabilities of point distribution and graph based methods are limited when neighboring points are close to each other [13] and have similar edge connections [14], respectively. Moreover, it is also difficult to achieve a good match under a single estimation for relatively large non-rigid distortions.

Iterative methods typically comprise an alternating two-step process: correspondence estimation and transformation updating. Compared with non-iterative methods, the key idea of iterative methods is to gradually adjust the initial geometrical structure and location of the source point set so that it becomes more similar to the target point set, and then correspondence estimation becomes easier. The TPS-RPM method [15] is one of the most notable

* Corresponding author at: School of Information Science and Technology, Yunnan Normal University, Kunming 650092, Yunnan, China. Tel.: +86 18987362208.

E-mail addresses: y.yang.tony@gmail.com (Y. Yang), eleongsh@nus.edu.sg (S.H. Ong), kelvinfoong@nus.edu.sg (K.W.C. Foong).

methods in this area. It employs softassign [16,17] and deterministic annealing [18,19] to estimate correspondences and control thin plate spline (TPS) [20] transformation updating, respectively. Recently Myronenko et al. [21] introduced a coherent points drift algorithm which is a maximum likelihood estimation with a motion coherence constraint [22] for preserving the topological structure of the point sets. Later, Myronenko and Song [23] (CPD) extended the former algorithm for both rigid and non-rigid registration, and provided a fast registration by using a fast Gauss transform [24] and low-rank matrix approximation [25]. More recently, Jian and Vemuri [14] (GMMREG) introduced a Gaussian mixture model approach for both rigid and non-rigid registration. They consider the registration problem as one of the aligning two Gaussian mixture models, and the transformation is updated by minimizing the L2 distance [26] between the two models.

Compared with TPS-RPM, CPD and GMMREG further improve transformation updating by using motion coherence and L2 distance minimization constraints, respectively. However, they still employ Gaussian probability density to assign their fuzzy correspondence which leads to ‘fuzzy location updating’ and requires relatively more iterations. Furthermore, forcing points to move coherently in CPD may produce position deviations of the rest of the points when one point is mismatched, and may also be undesirable when source points need to be moved in different directions to match their target points at the same time. In addition, the Euclidean distance between two point sets in GMMREG is not always minimized by minimizing the L2 distance between two Gaussian mixture models.

In this work, we present a global and local mixture distance (GLMD) based non-rigid point set registration method which belongs to the aforementioned iterative methods. The method first defines two distance features (global and local distances) for measuring global and local structural differences between two point sets, respectively. The two distances are then combined to form a GLMD based cost matrix, which provides a flexible way to estimate the correspondence by minimizing the local or global structural difference between the two point sets using a linear assignment solution. To improve the correspondence estimation by using both local and global distance features and enhance the interaction between the two steps, an annealing scheme is designed to smoothly control the minimization balance of the GLMD cost matrix and the rigid and non-rigid transformations of the TPS. These optimized controls cause the registration process to first focus on searching local structural similarities (by minimizing the local distance) between two point sets with the TPS performing a more rigid transformation at the start of registration, followed by minimizing the global structural difference (by minimizing the global distance) between the two point sets with the TPS performing a more non-rigid transformation at the end of registration.

Compared with the current methods, the major differences and advantages of this work include: (i) we improve the flexibility and accuracy of correspondence estimation by using multi-feature based correspondence estimation; (ii) we preserve the topological structure of the point sets by maintaining neighboring relations of points (through minimizing the local distance); (iii) the defined local distance provides a more flexible parameter setting for dealing with registrations under different levels of deformation, noise, outliers, rotation and missing points; (iv) the Euclidean distance between two point sets is always minimized by the subsequent global distance minimization; (v) we enhance the interaction between correspondence estimation and transformation updating by first minimizing the local structural differences with more rigid transformations and then minimizing the global structural differences with more non-rigid transformations.

The rest of the paper is organized as follows: in Section 2, we present the main ideas of this work and discuss related work and

the advantages of our method; in Section 3, we evaluate the performances of our method in contour registration, sequence images and real images, and its comparisons with six state-of-the-art methods (TPS-RPM [15], CPD [23], GMMREG [14], Caetano et al. [9,10], FGM [11] and Leordeanu et al. [12]) are also demonstrated; in Section 4, we conclude with a discussion.

2. Method

We first define global, local and mixture distances, and introduce the main process of our method. The free parameter setting in our method and the differences between our method and related work are discussed in the latter part of this section.

2.1. Global, local and mixture distances

2.1.1. Global distance

Global distance is used to measure squared Euclidean distances from one point set to another, and defined as

$$\mathbf{G}_{a_i b_j} = G(\mathbf{a}_i, \mathbf{b}_j) = \|\mathbf{a}_i - \mathbf{b}_j\|^2 \quad (1)$$

where the matrix \mathbf{G}_{ab} describes the global structural difference between point set \mathbf{a} and point set \mathbf{b} . If we consider \mathbf{G}_{ab} as a global cost matrix and minimize it by a linear assignment solution, we will obtain the corresponding relation between \mathbf{a} and \mathbf{b} , which is based on the minimization of global structural difference between the two point sets.

2.1.2. Local distance

Local distance is designed to measure local differences (or similarities) from one point set to another. The basic idea is shown in Fig. 1.

For example, in order to find a corresponding segment A' for A , we first translate the five neighboring points of the center point (the red point in Fig. 1) in A to each A' according to a displacement vector from the center point in A to the center point in A' . Then, we sum the distances between the two sets of neighboring points. Finally, the corresponding segment of A is determined by a segment having the shortest summed distance. The local distance is formulated as

$$\mathbf{L}_{a_i b_j} = L(\mathbf{a}_i, \mathbf{b}_j) = \sum_{k=1}^K \|T(\mathbf{N}(\mathbf{a}_i)_k, \mathbf{b}_j) - \mathbf{N}(\mathbf{b}_j)_k\|^2 \quad (2)$$

where \mathbf{L}_{ab} is a local distance matrix from point set \mathbf{a} to point set \mathbf{b} , and K is the number of neighboring points. $\mathbf{N}(\mathbf{a}_i)_k$ and $\mathbf{N}(\mathbf{b}_j)_k$ are the k th closest point for the points \mathbf{a}_i and \mathbf{b}_j , respectively. T is the translation function defined by

$$T(\mathbf{N}(\mathbf{a}_i)_k, \mathbf{b}_j) = \mathbf{N}(\mathbf{a}_i)_k + (\mathbf{b}_j - \mathbf{a}_i) \quad (3)$$

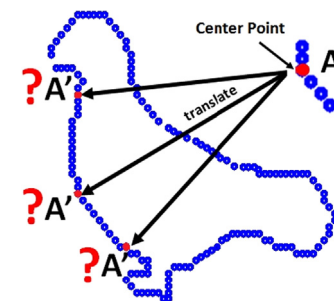


Fig. 1. Local similarity measurement. Each red point and its neighboring points (the five points) construct a small segment in the point set, such as A and A' shown here. (For interpretation of the references to color in this figure caption, the reader is referred to the web version of this article.)

The local distance $L(\mathbf{a}_i, \mathbf{b}_j)$ is mainly determined by the number of neighboring points K which plays an important role in measuring local similarity, preserving the topological structure of the point sets as well as dealing with noise, outliers, rotation and missing points. Here, if we consider \mathbf{L}_{ab} as a local cost matrix and minimize it by a linear assignment technique, we will obtain the corresponding relation between \mathbf{a} and \mathbf{b} , which is based on the minimization of local structural differences between the two point sets.

2.1.3. Mixture distance

The mixture distance consists of the global and local distance matrices. It is defined as

$$\mathbf{C}_{ab} = \mathbf{G}_{ab} + \alpha \cdot \mathbf{L}_{ab} \quad (4)$$

where \mathbf{C}_{ab} is a GLMD based cost matrix. α is a weighting parameter that controls the balance between the global and local costs in \mathbf{C}_{ab} . For example, when α is very large, minimizing \mathbf{C}_{ab} is equal to minimizing the local distance cost \mathbf{L}_{ab} . The process tends to minimize the global distance cost \mathbf{G}_{ab} when α becomes small. The designed mixture distance \mathbf{C}_{ab} provides a flexible way to estimate the correspondence by minimizing the local or global structural difference between two point sets.

2.2. Main process

Suppose we have two point sets $\{\mathbf{x}_i, i=1, 2, \dots, X\}$ and $\{\mathbf{y}_j, j=1, 2, \dots, Y\}$ in R^2 or in R^3 for the source point set \mathbf{x} and the target point set \mathbf{y} , respectively. The process of this method is first (i) to use a warping template \mathbf{x}^w (the initial $\mathbf{x}^w = \mathbf{x}$) to estimate corresponding points \mathbf{y}^c (the points in \mathbf{y}) for \mathbf{x} at each iteration, and then (ii) to update the locations of \mathbf{x}^w using the recovered correspondence between \mathbf{x} and \mathbf{y}^c . The steps (i) and (ii) are iterated such that the warping template \mathbf{x}^w can gradually and continuously approach the target point set \mathbf{y} , and finally match the exact corresponding points in \mathbf{y} .

2.2.1. Correspondence estimation

The list of corresponding points \mathbf{y}^c at each iteration is estimated by minimizing the total cost function

$$C_{\text{total}}(\mathbf{M}) = \sum_i^X \sum_j^Y \mathbf{M}_{ij} \mathbf{C}_{x_i^w y_j} \quad (5)$$

where the solution \mathbf{M} is a binary correspondence matrix (from \mathbf{x}^w to \mathbf{y}) and still satisfies $\sum_j^Y \mathbf{M}_{ij} = 1$ for $i \in 1, \dots, X$ with $\mathbf{M}_{ij} \in 0, 1$. $\mathbf{C}_{x^w y}$ is the GLMD based cost matrix (described in Section 2.1.3) from \mathbf{x}^w to \mathbf{y} . $\mathbf{C}_{x^w y}$ contains the weighting parameter α that is controlled by an annealing scheme for changing the minimization from the local distance to the global distance. For each point \mathbf{x}_i^w and \mathbf{y}_j , the sets of neighboring points $\mathbf{N}(\mathbf{x}_i^w)$ and $\mathbf{N}(\mathbf{y}_j)$ used in the local distance $\mathbf{L}_{x^w y}$ are determined by the Euclidean distance relationships in the source point set \mathbf{x} and the target point set \mathbf{y} , respectively. Since a local distance $L(\mathbf{x}_i^w, \mathbf{y}_j)$ is measured from two small segments and the determined neighboring relations $\mathbf{N}(\mathbf{x}_i^w)$ and $\mathbf{N}(\mathbf{y}_j)$ are fixed during the warpings of \mathbf{x}^w , minimizing the local distance preserves the topological structures of the point set \mathbf{x}^w .

To find the correspondence matrix \mathbf{M} where the total cost C_{total} has the minimum value, we solve the total cost function as a linear assignment problem by using the Jonker–Volgenant algorithm [27] which provides the shortest augmenting path and has worst-cost time $O(N^3)$. The original Jonker–Volgenant algorithm was developed for integer cost and only works on the square cost matrix. To overcome the two limitations, the calculated GLMD based cost $\mathbf{C}_{x^w y}$ is rounded by $\lfloor \mathbf{C}_{x^w y} \times R \rfloor$ where R is a large resolution and set to 10^6 (since we rescale the coordinates of all

points within (0,1) before registration) in this work. If the size of point set \mathbf{x} is less than point set \mathbf{y} (\mathbf{y} includes outliers or \mathbf{x} misses points), the non-square cost $\mathbf{C}_{x^w y}$ will be converted into a square cost problem by assigning dummy entries [28] that do not affect the total cost. $\mathbf{C}_{x^w y}$ can then be solved in the usual way and still give the best solution. The solved M guarantees one-to-one correspondence (from \mathbf{x}^w to \mathbf{y}). The new correspondence \mathbf{y}^c for the \mathbf{x} is then updated by

$$\mathbf{y}^c = \mathbf{M} \cdot \mathbf{y} \quad (6)$$

2.2.2. Transformation updating

After updating \mathbf{y}^c , the spatial transformation is refined by the current correspondence \mathbf{y}^c and the source point set \mathbf{x} . In this work, we map \mathbf{x} to \mathbf{y}^c by TPS transformation

$$f(\mathbf{x}, \mathbf{d}, \mathbf{w}) = \mathbf{x} \cdot \mathbf{d} + \phi(\mathbf{x}) \cdot \mathbf{w} \quad (7)$$

where \mathbf{d} is an affine coefficient matrix and \mathbf{w} is a non-rigid warping coefficient matrix. $\phi(\mathbf{x})$ is the TPS kernel defined by $\phi(\mathbf{x}) = \|\mathbf{x} - \mathbf{x}_c\|^2 \log \|\mathbf{x} - \mathbf{x}_c\|$ and $\phi(\mathbf{x}) = \|\mathbf{x} - \mathbf{x}_c\|$ for the 2D and 3D cases, respectively. \mathbf{x}_c is a set of control points chosen from \mathbf{x} .

To map \mathbf{x} to its correspondence \mathbf{y}^c with the proper \mathbf{d} and \mathbf{w} , the TPS energy is defined as

$$E_{\text{TPS}}(f) = \sum_{i=1}^X \|\mathbf{y}^c - f(\mathbf{x})\|^2 + \lambda \iint \left[\left(\frac{\partial^2 f}{\partial x^2} \right)^2 + 2 \left(\frac{\partial^2 f}{\partial x \partial y} \right)^2 + \left(\frac{\partial^2 f}{\partial y^2} \right)^2 \right] dx dy \quad (8)$$

By substituting the solution for Eq. (7) into Eq. (8), the TPS energy function becomes

$$E_{\text{TPS}}(\mathbf{d}, \mathbf{w}) = \|\mathbf{y}^c - \mathbf{x} \cdot \mathbf{d} - \Phi \mathbf{w}\|^2 + \lambda \text{tr}(\mathbf{w}^T \Phi \mathbf{w}) \quad (9)$$

where the regularization parameter λ penalizes the non-rigid warping coefficient \mathbf{w} , and is controlled by the same annealing scheme applied to the aforementioned weighting parameter α in Eq. (4). Φ is the kernel matrix from the kernel function $\phi(\mathbf{x})$.

To find the least-squares solutions for the \mathbf{d} and \mathbf{w} , the QR decomposition [29] is used to separate the affine and non-rigid warping space by

$$\mathbf{x} = \mathbf{Q} \mathbf{R} = [\mathbf{Q}_1 | \mathbf{Q}_2] \begin{pmatrix} \mathbf{R}_1 \\ 0 \end{pmatrix} \quad (10)$$

where \mathbf{Q}_1 is an $N \times D$ matrix, \mathbf{Q}_2 is $N \times (N-D)$, \mathbf{R}_1 is $D \times D$, and \mathbf{Q}_1 and \mathbf{Q}_2 both have orthogonal columns. Thus (9) becomes

$$E_{\text{TPS}}(\mathbf{y}, \mathbf{d}) = \|\mathbf{Q}_2^T \mathbf{y}^c - \mathbf{Q}_2^T \Phi \mathbf{Q}_2 \mathbf{y}\|^2 + \|\mathbf{Q}_1^T \mathbf{y}^c - \mathbf{R}_1 \mathbf{d} - \mathbf{Q}_1^T \Phi \mathbf{Q}_2 \mathbf{y}\|^2 + \lambda \mathbf{y}^T \mathbf{Q}_2^T \Phi \mathbf{Q}_2 \mathbf{y} \quad (11)$$

where $\mathbf{w} = \mathbf{Q}_2 \mathbf{y}$ and \mathbf{y} is $(N-D-1) \times (D+1)$. The least-squares solution for Eq. (11) can first be minimized with respect to \mathbf{y} and then with respect to \mathbf{d} . The final solutions for \mathbf{w} and \mathbf{d} are

$$\hat{\mathbf{w}} = \mathbf{Q}_2 \mathbf{y} = \mathbf{Q}_2 (\mathbf{Q}_2^T \Phi \mathbf{Q}_2 + \lambda \mathbf{I}_{N-D-1})^{-1} \mathbf{Q}_2^T \mathbf{y}^c \quad (12)$$

$$\hat{\mathbf{d}} = \mathbf{R}^{-1} (\mathbf{Q}_1^T \mathbf{y}^c - \Phi \mathbf{w}) \quad (13)$$

The new location of the warping template \mathbf{x}^w is updated by

$$\mathbf{x}^w = \mathbf{x} \cdot \mathbf{d} + \Phi \cdot \mathbf{w} \quad (14)$$

After updating the location of \mathbf{x}^w , we return to the first step (Section 2.2.1) and continue the registration process until the final temperature T_{final} of the annealing scheme is reached.

2.3. An annealing scheme

Deterministic annealing [18,19] is a useful heuristic to avoid local minima for a variety of optimization problems, and has proven to be especially successful in dealing with difficult combinatorial optimization problems [30,15,21,14]. An annealing scheme (i.e., an annealing

parameter T) starts with a high temperature T_{init} , and ends with a specified low temperature T_{final} . T is gradually reduced by a linear annealing schedule $T = T \cdot r$ where r is the annealing rate. The main reasons for using an annealing scheme in this work are: (i) to reduce the parameter α ($\alpha = \alpha_{init} \cdot T$) in Eq. (4) so as to change the cost minimization from local to global, and (ii) to reduce the parameter λ ($\lambda = \lambda_{init} \cdot T$) in Eq. (12) so as to adjust the TPS transformation from rigid to non-rigid.

For example, at the start of registration, a large initial α_{init} causes the correspondence matrix to focus on searching local similarities between \mathbf{x}^w and \mathbf{y} . Minimizing the local distance preserves the topological structure of the warping template \mathbf{x}^w and deals with noise, outliers, rotation and missing points. It also improves the correspondence estimation, while the improved recovered correspondences make the TPS transformation better behaved. Furthermore, with a large λ , the TPS performs a more rigid transformation and also preserves the topological structure of \mathbf{x}^w , prevents mismatches and rejects noise and outliers. As the temperature T decreases, α and λ become small. The registration process tends to minimize the global distance between \mathbf{x}^w and \mathbf{y} , while the TPS performs a more non-rigid transformation to make \mathbf{x}^w approach \mathbf{y} as close as possible.

To summarize, the minimum energy of the TPS obtained at each temperature (i.e., at each iteration) is used as initial condition for the next iteration such that the registration process can avoid many local minima to finally find a good approximation to the global minima of the mapping and the correspondence. Furthermore, the annealing scheme combined with the GLMD based cost matrix improves the flexibility and accuracy of the correspondence estimation by using both local and global distance features, and also enhances the interaction between the two steps during the registration.

2.4. Our algorithm and parameter setting

The pseudo code of our method is shown in [Algorithm 1](#) (referred to as GLMDTPS). There are four groups of free parameters in our method: the annealing parameters T_{init} , T_{final} and r , the weighting parameter α , the regularization parameters λ , and the number of neighboring points K .

- **Annealing parameters:** T_{init} , T_{final} and r are set to ensure there are sufficient iterations for the registration process. Based on an initial trial-and-error experiment using Fish1, T_{init} is set to 1/10 of the largest squared distance between x and y , T_{final} is chosen to be equal to 1/8 of the mean squared distance between the neighboring points in x , and r is usually set to 0.7.
- **Weighting parameter:** The value of α_{init} is large to make the correspondence estimation focus on minimizing local differences at the start of registration. The initial value of α_{init} is set to the squared number of the neighboring points K^2 .
- **Regularization parameter:** The value of λ_{init} is large to make the TPS focus on performing more rigid transformations at the start of registration. The initial value of λ_{init} is set to the length of point set x .
- **The number of neighboring points:** The value of K is based on the minimum number of points used for distinguishing local structures. For example, to distinguish between a corner (includes two neighboring points) and a cross (includes four neighboring points), at least four neighboring points are required. K is set to 5 for both 2D and 3D as default. It can also be optimized for a particular case since adjusting the number of neighboring points can better distinguish local structures for improving the correspondence estimation and dealing with noise, outliers and rotation (see [Section 3.1.4](#)).

Algorithm 1. GLMDTPS.

Input: Point sets x and y
To initialize parameters T_{init} , T_{final} , r , λ_{init} and α_{init}
To set K and determine $N(\mathbf{x}_i^w)_k$ and $N(\mathbf{y}_i)_k$ for \mathbf{x}^w and y
Begin I: Annealing scheme
Step 1: Estimating the current correspondences \mathbf{y}^c by Eqs. (5) and (6).
Step 2: Updating the TPS transformation by Eqs. (12) and (13).
Update the location of \mathbf{x}^w by Eq. (14).
Update the parameter α and λ by decreasing T .
End I: Until $T \leq T_{final}$ is reached.
Output: Warped source point set \mathbf{x}^w

2.5. Related work and advantages

There are three aforementioned methods: TPS-RPM [15], CPD [23] and GMMREG (L2+TPS) [14] that are generally related to our method. The methodological differences between our method and the other three methods ([Table 1](#)) and the significant advantages of our method are described as follows:

- **Correspondence estimation:** Unlike single feature based correspondence estimations in the current methods, we minimize a multi-feature (i.e., GLMD) based cost matrix by a linear assignment solution which provides a binary correspondence and guarantees one-to-one correspondence. Moreover, the correspondence estimations in the other three methods are determined by a fuzzy correspondence using Gaussian probability density that is mainly related to $\|\mathbf{x}_i^w - \mathbf{y}_j\|^2$ as our defined global distance. Compared with the three methods, the defined local distance feature is more stable and robust (than $\|\mathbf{x}_i^w - \mathbf{y}_j\|^2$) for correspondence estimation at the beginning of registration, and helps the warping template more quickly (using fewer iterations) achieve a better pose for the subsequent more non-rigid registration. To avoid mismatches by neighboring points having similar local structures (such as the aforementioned limitations in point distribution and graph based methods), minimizing the local distance is replaced by minimizing the global structure difference at the end of registration, which always minimizes the Euclidean distance between two point sets (i.e., it solves the issue in GMMREG).
- **Transformation updating:** Our method and TPS-RPM minimize TPS energy to update the transformation. However, TPS-RPM employs an additional penalty term $\lambda_2 \text{tr}[d - I]^T[d - I]$ for the affine coefficient \mathbf{d} . We only penalize the non-rigid warping coefficient \mathbf{w} since our method returns a relatively accurate

Table 1

Methodological differences between our method and current methods. GPD: Gaussian probability density; GLMD: global and local mixture distance; B: binary; F: fuzzy; GRBF: Gaussian radial basis function; TPS: thin plate spline; MCC-NLL: motion coherence constraint based negative log-likelihood; Mini-L2: minimizing L2 distance. Note that a term $\lambda_2 \text{tr}[d - I]^T[d - I]$ is added to TPS Energy2 to Eq. (9) for penalizing the affine transformation.

Methods	Correspondence estimation		Transformation update	
	Using feature	Correspondence	Constraint	Transformation
GLMDTPS	GLMD	B	TPS Energy1	TPS
TPS-RPM	GPD	F	TPS Energy2	TPS
CPD	GPD	F	MCC-NLL	GRBF
GMMREG	GPD	F	Mini-L2	TPS

- binary correspondence to the transformation at each iteration, and hence a free affine transformation will be helpful to quickly (using fewer iterations) achieve a better pose (\mathbf{x}^w) for the subsequent more non-rigid registration.
- *Fuzzy correspondence vs. Binary correspondence:* The transformations built by the fuzzy correspondences in the three methods give fuzzy location and geometrical structure updating for the warping template. These may cause the registration process to take relatively more iterations and not be always effective for the warping template updating. In our method, the series of binary correspondences estimated by the defined local distance feature clearly guide the location and geometrical structure updating with rigid transformations at the beginning of registration. Consequently, the achieved better pose makes the subsequent correspondence estimation using the global distance feature easier.
 - *Topological structure:* Unlike forcing points to move coherently in the CPD, we fix neighboring relations $\mathbf{N}(\mathbf{x}_i^w)$ and $\mathbf{N}(\mathbf{y}_j)$ during the warpings of \mathbf{x}^w . Thus, minimizing the local distance preserves the topological structure of the warping template, while also avoiding the position deviations issues such as in CPD.
 - *Flexibility:* The TPS-RPM and CPD methods consider the outlier rejection as an unsupervised clustering problem, and the GMMREG rejects outliers by its defined Gaussian component which is mainly related to the Mahalanobis distance [31]. In our method, the local distance determines the measurements of local similarities between two point sets, and provides an adjustable parameter K (the number of neighboring points) for flexibly dealing with registrations under different levels of deformation, noise, outliers, rotation and missing points.
 - *Interaction between two steps:* The annealing scheme combined with the GLMD based cost matrix improves the flexibility and accuracy of the correspondence estimation by using both local and global distance features, and also enhances the interaction between the two steps during registration (as described in Section 2.3).

3. Experiments

We implemented the main process of our method in Matlab, and the Jonker-Volgenant algorithm in C++ as a Matlab mex function. We tested the performances of our method in three series of experiments

- Contour registration
- Sequence images
- Real images

and compared against three types of state-of-the-art methods:

- Iterative methods: TPS-RPM [15], CPD [23] and GMMREG [14].
- Non-learning graph based methods: FGM [11].

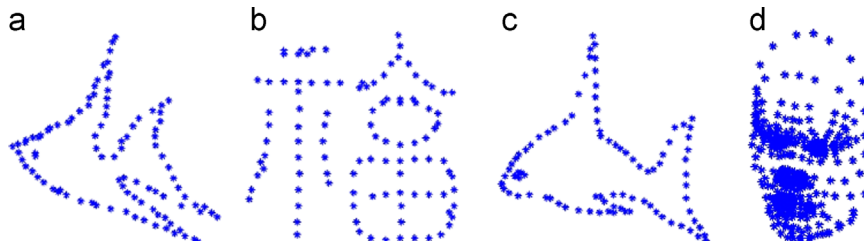


Fig. 2. TPS-RPM and CPD testing point sets: (a) Fish1 (98 points), (b) Chinese Character (105 points), (c) Fish2 (91 points) and (d) Face3D (392 points). (a) and (b) are obtained from Chui and Rangarajan [15]. (c) and (d) are obtained from Myronekon and Song [23].

- Learning graph based methods: Caetano et al. [9,10] and Leordeanu et al. [12].

In addition, we also evaluated the computational complexity of our method, and discussed how the computational cost can be reduced.

3.1. Experiments on contour registration

In the first series of experiments, we evaluate the performances of our method on different contour registration problems. Compared with the labeled feature point sets in sequence images and real images (such as CMU sequence and Pascal 2007 challenge), contour point sets are typically sampled by a relatively high sampling rate and distinguishing local similarities is more difficult since contour points are very close to each other and have similar local features.

3.1.1. Performance on four popular point sets

There is no standard contour database that has been commonly used for experimental comparison by different methods. We first select the four most popular point sets from the TPS-RPM and CPD work (Fig. 2).

Experiment design: To generate a series of ‘moderate’ and ‘rich’ target point sets from the selected point sets, we design the experiments as follows

- (a) *Deformation:* Eight control points on the boundary of each source point set (six control points on the left, right, anterior, posterior, superior and inferior of the boundary for 3D) are set as shown in Fig. 3. Each control point is set with four free moving directions (nine directions for 3D) and a displacement of 0.2. The order and the moving directions of control points are randomly determined. TPS transformation is employed to warp source point sets using the defined control points, and

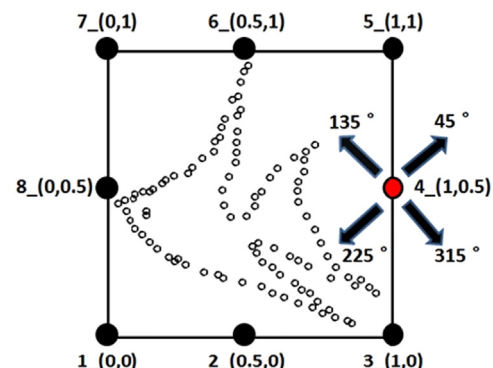


Fig. 3. Deformation experiment design.

Table 2

Parameter setting for each method. Init: the initial parameter setting described in Section 2.4. P1: $\lambda = 2$ and $\beta = 2$ for deformation and rotation experiments. P2: $\lambda = 2$ and $\beta = 3$ for deformation and rotation experiments. P3: $\lambda = 2$, $\beta = 2$ and $\omega = 0.3$ for noise and outlier experiments. P4: $\lambda = 2$, $\beta = 2$ and $\omega = 0.5$ for noise and outlier experiments. P5: $\lambda = 2$, $\beta = 3$ and $\omega = 0.4$ for noise and outlier experiments. P6: $i_1^{init} = 1$, $i_2^{init} = 0.01$, $r = 0.93$, and T_{init} and T_{final} are set to the largest square distance of all point pairs and the average of the squared distance between the nearest neighbors within the set of points which are being deformed, respectively. P7: L2-TPS [23]. \times : no parameter value was provided for the point set.

Setting	Fish1	Chinese Character	Fish2	Face3D
GLMDTPS	Init	Init	Init	Init
CPD	P1, P3	\times	P1, P4	P2, P5
TPS-RPM	P6	P6	\times	\times
GMMREG	P7	\times		P7

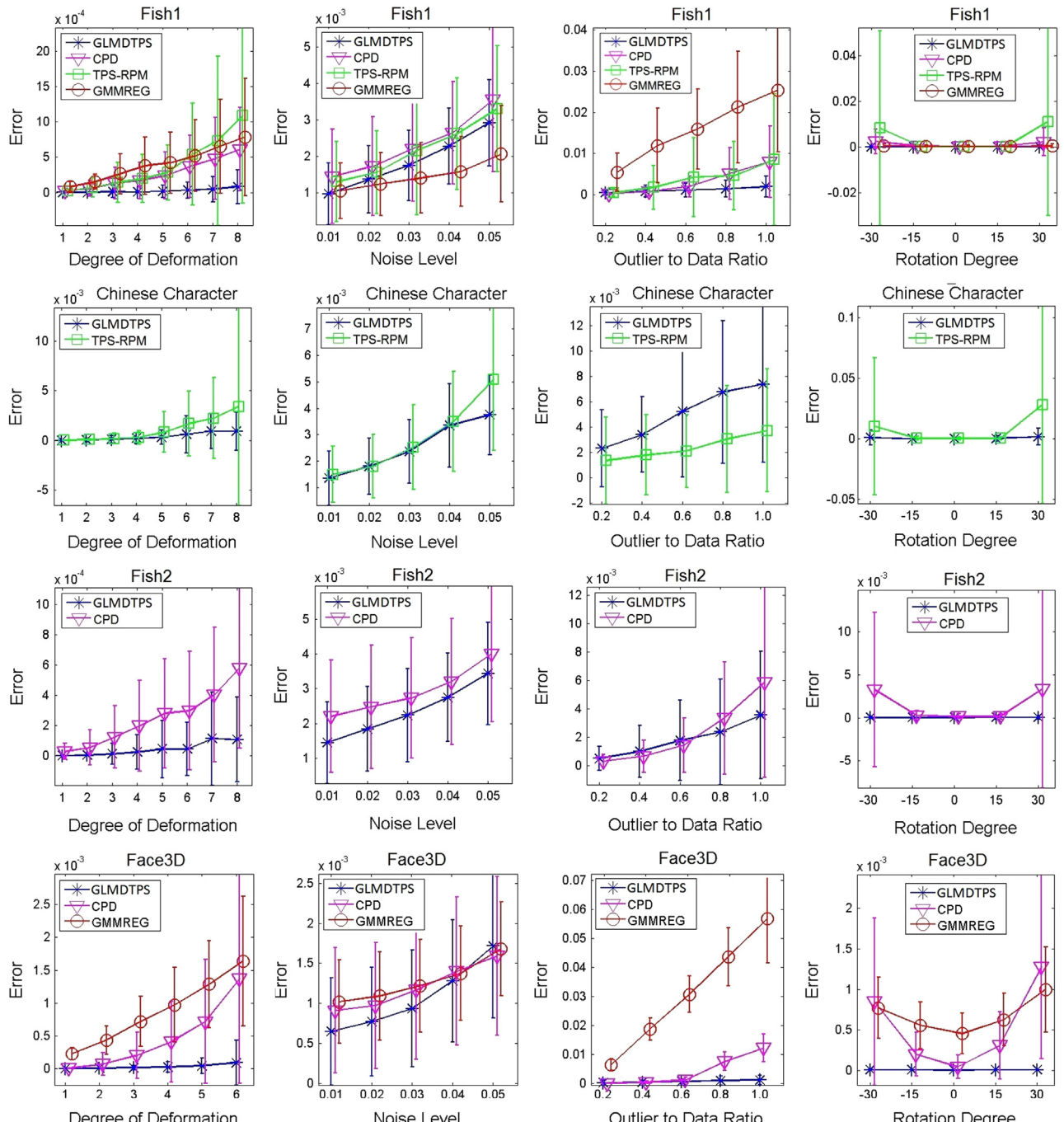


Fig. 4. Comparison of our results (*) against CPD (\triangledown), TPS-RPM (\square) and GMMREG (\circ) on the four point sets. The error bars indicate the standard deviations of the mean errors in 100 random experiments. From the top row to bottom row are: Fish1, Chinese Character, Fish2 and Face3D, respectively.

the order of the warped source points is then randomly rearranged. The degree of deformation is defined as the number of moved control points since the higher level of point perturbations produces higher deformation.

- (b) *Noise*: Five noise levels are used and defined as Gaussian white noise with a zero mean and standard deviation from 0.01 to 0.05.
- (c) *Outlier*: Five outlier to data ratios are used and defined as the outlier to original data ratios ranging from 0.2 to 1.
- (d) *Rotation*: We focus on the rotation range from -30° to 30° with a 15° interval (the target point sets in 3D case are rotated on the vertical axis) since beyond this range some methods will show an unstable performance. Although the other three methods have not been evaluated in non-rigid rotation experiments, we consider that evaluating performance under moderate rotations is essential since the deformation is often accompanied by a rotation.

For (b) (c) and (d), each source point set is also randomly warped by a medium degree of deformation (the fourth degree for 2D and the third degree for 3D) before adding noise, outliers or rotations.

Performance assessment: In order to achieve a direct and fair comparison with the other three methods, we followed the same error measurement and the overall performance assessment in TPS-RPM [15] and CPD [23]: the mean squared distance between the recovered corresponding points and the exact corresponding points, and the mean error. For each point set, one hundred random experiments are repeated for each setting (i.e., each

degree of deformation, noise level, outlier ratio and rotation degree) in each experiment.

Comparison approach: In the first experiment, we only compared the performance of our method against the others under their already tested point sets since they only provided the parameter values (in the published papers [15,23,14] and the source codes [32–34]) for those point sets as shown in Table 2. The parameters of our method are set as described in Section 2.4. The comparison results are shown in Fig. 4 and discussed as follows:

- *Fish1*: The performance statistics (the mean error and its standard deviation) are shown in the first row of Fig. 4. Our method shows accurate alignments in all experiments, and gives the best performances over all degrees of deformation, outlier to data ratios from 0.6 to 1.0, and all degrees of rotation. In the noise experiment, all the four methods give accurate alignments while GMMREG generally performed better. Registration examples are shown in Fig. 5.
- *Chinese character*: We only present the performances of our method and TPS-RPM in this experiment (the second row of Fig. 4) since Chinese Character has not been tested in the CPD and GMMREG papers for non-rigid point set registration (GMMREG only tested it in the rigid registration experiment). Our method shows accurate alignments and gives the best performances over all degrees of deformation, all noise levels and all degrees of rotation. In the outlier experiment, TPS-RPM performs better. The reason why our method performed

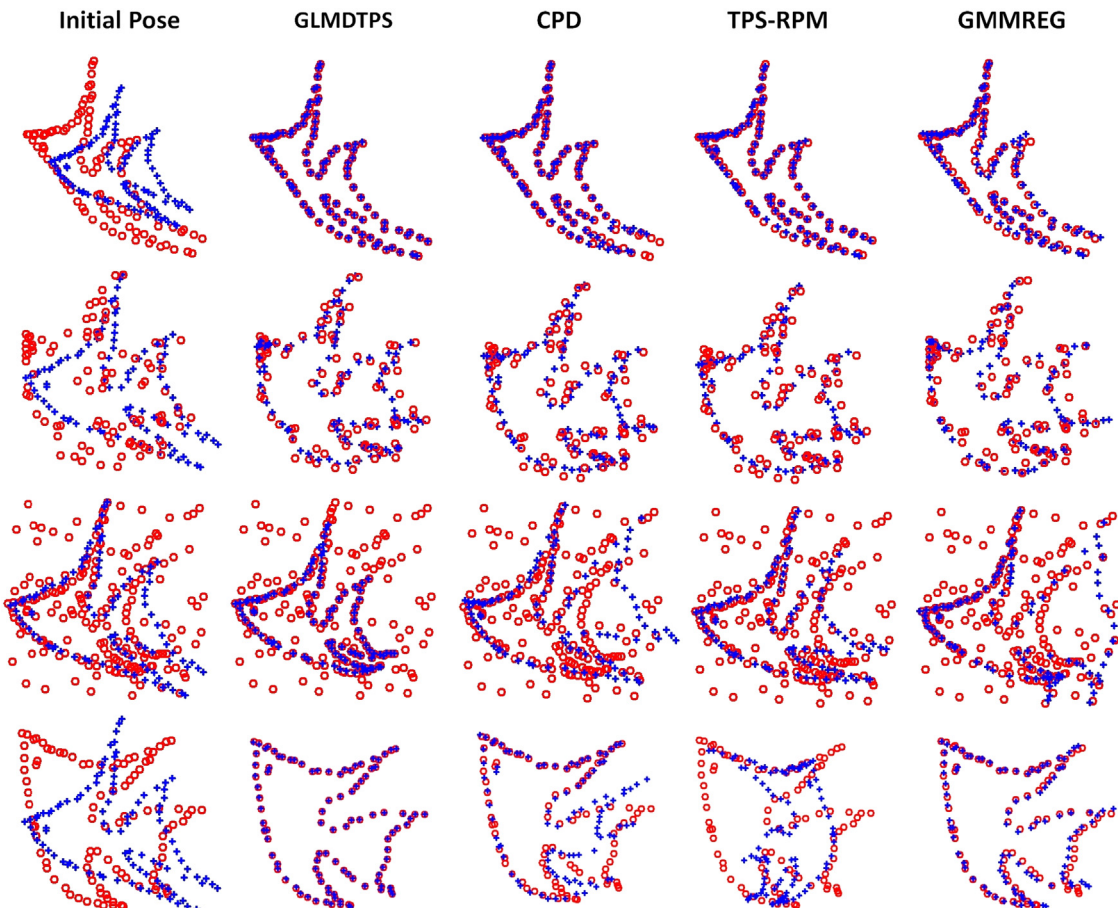


Fig. 5. Registration examples on Fish1. From the top row to bottom row are examples in the deformation (the 8th degree), noise (0.03), outlier (1.0) and rotation (-30°) experiments.

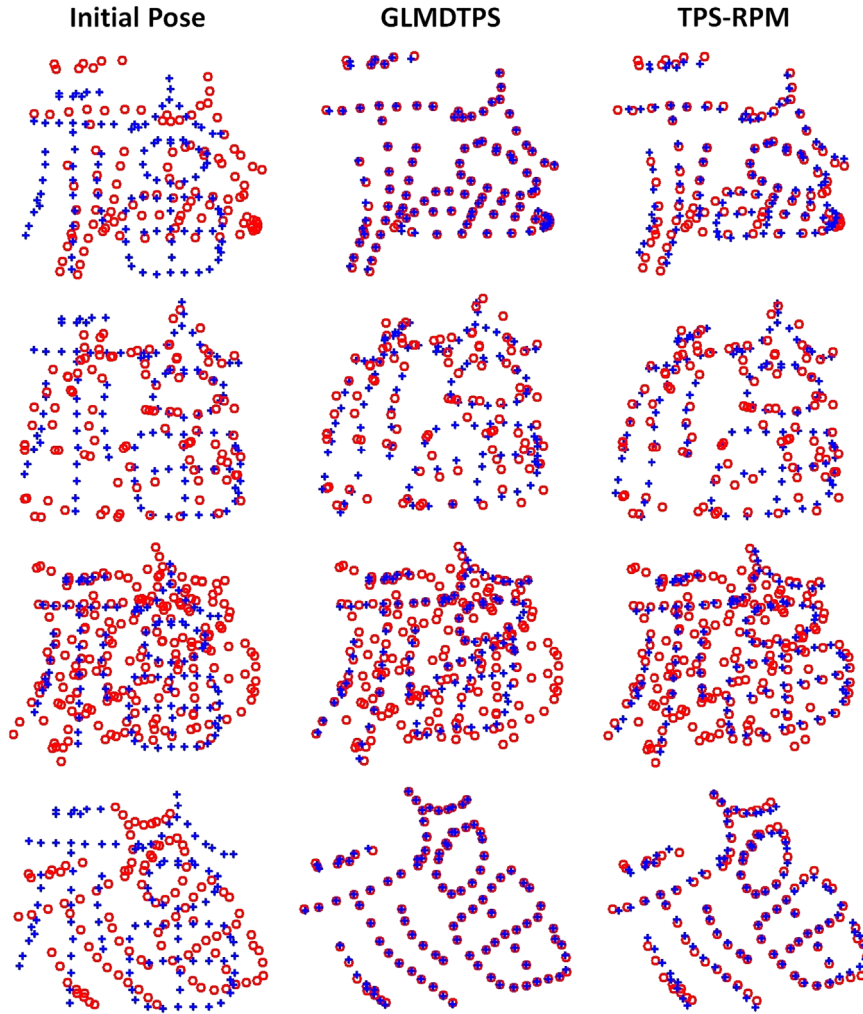


Fig. 6. Registration examples on Chinese Character. From the top row to bottom row are examples in the deformation (the 8th degree), noise (0.03), outlier (1.0) and rotation (30°) experiments.

relatively poorly is that the outliers spreading out on the Chinese Character shape can easily change the local structures compared with the other point sets such as Fish1. Registration examples are shown in Fig. 6.

- **Fish 2:** The performances of our method and CPD are given in the third row of Fig. 4. Our method shows accurate alignments in all experiments, and gives the best performances over all degrees of deformation, all noise levels, large outlier ratios from 0.8 to 1.0, and all degrees of rotation. Registration examples are shown in Fig. 7.
- **Face 3D:** The performances of our method, CPD and GMMREG are given in the fourth row of Fig. 4. Our method shows accurate alignments in all experiments, and gives the best performances over deformation degrees from the second to the eighth degrees, noise levels from 0.01 to 0.04, outlier ratios from 0.6 to 1.0, and all degrees of rotation. Registration examples are shown in Fig. 8.

3.1.2. Performance on a wide range of geometrical shapes

In this experiment, we consider that a good non-rigid point set registration method should be robust to different geometrical shapes and not be sensitive to its parameter setting since we normally deal with a non-rigid point set registration as an unknown problem where we may not be allowed to tweak parameter values for each case. Thus, we further add another five

point sets (shown in Fig. 9), and combine them with the Fish1 and Chinese Character point sets to evaluate the performances of the four methods. The parameter setting of each method followed the same setting in the Fish1 experiment.

The mean performances (i.e., the mean error) of the four methods on the seven point sets are shown in Fig. 10. Our method shows accurate alignments in all experiments, and gives the best performances over all degrees of deformation, noise levels from 0.01 to 0.03, outlier to data ratios from 0.8 to 1.0 and all degrees of rotation. To quantify the comparison results, we score the performances from the best to the worst in each setting of each point set (e.g., the first degree of deformation in the Line point set experiment) using ordinal ranking 4, 3, 2, 1 according to the calculated errors of the four methods. The summed scores and the mean scores are shown in Table 3. The results verify that our method is robust to different geometrical shapes and is stable to the initial parameter values. Furthermore, our method gives the best overall performances in the deformation, noise and rotation experiments, and very similar performance to the CPD which performs best in the outlier experiments. Registration examples are shown in Fig. 11.

3.1.3. Performance on partial matching

There are typically two types of partial matching: missing points on one side and on both sides. Our method is robust to

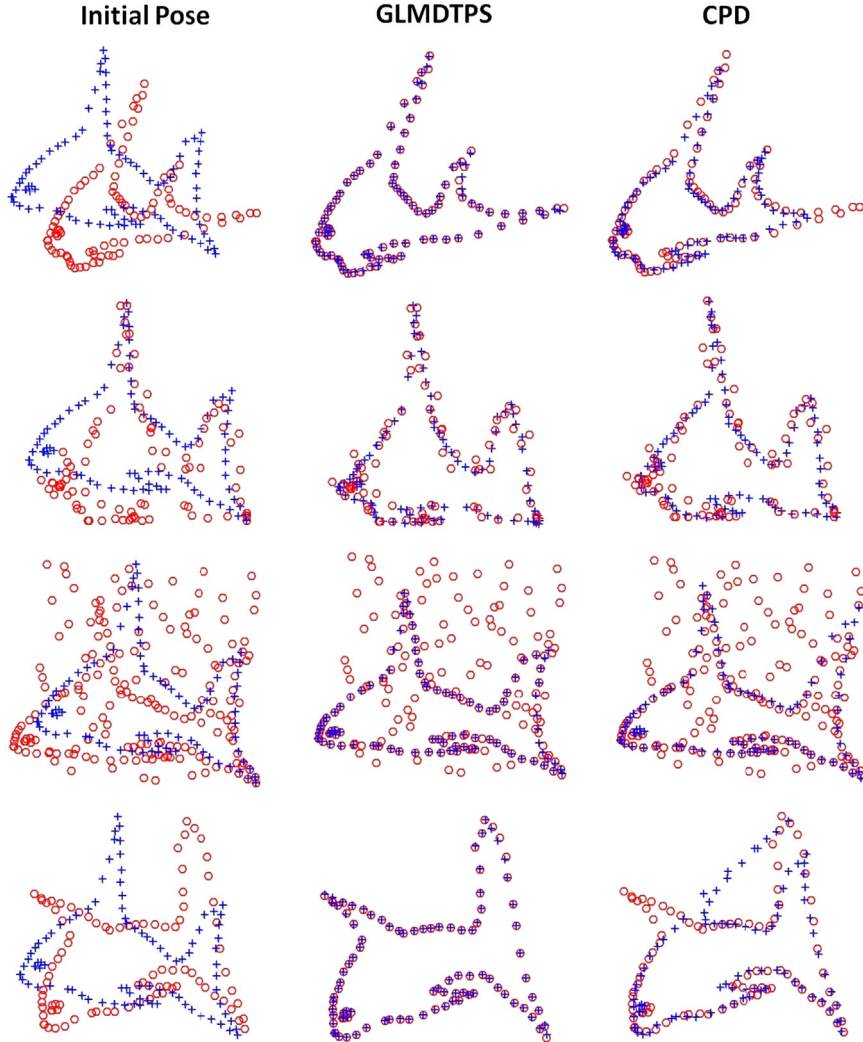


Fig. 7. Registration examples on Fish2. From the top row to bottom row are examples in the deformation (the 6th degree), noise (0.03), outlier (1.0) and rotation (30°) experiments.

the first case, but may not be able to cope well with missing points on both sides since it forces one-to-one correspondence even if corresponding points (in the target point set) do not exist. The performances of the four methods with missing points on the source point set are shown in Fig. 12(a). The location of missing part was randomly determined, while the target point set was also randomly warped by the fourth degree of deformation. One hundred random experiments were repeated for each missing point ratio setting. Our method gives the best performances over all the ratios, and shows very accurate results (Error < 0.0019) when the ratio is below 0.5. Registration examples are shown in Fig. 12(b).

3.1.4. Performance with variable numbers of neighboring points

The number of neighboring points K plays an important role in measuring local similarity, preserving topological structure and dealing with noise, outliers and rotation during registration. Adjusting the number of neighboring points makes our method better behaved. In this section, we give several examples in improving the performance of our method by adjusting the number of neighboring points.

High sampling rate case: Many studies in medical imaging sought to use more sampling points to align two shape models for observing

local differences such as muscle deformation [35–38], stomach deformation [39], breathing motion [40], brain mapping [41] and animal skeleton [13]. In these cases, a small local segment in a point set is represented by more points. Thus increasing the number of neighboring points will help to improve the local similarity measurement. A point set (Bird2) with 1715 points, which has a similar geometrical shape to Bird1 but with more details in its feet and tail, is used in this experiment. To select a proper K for this point set, we tested the performances with different numbers of neighboring points on the former seven point sets. For each point set, we start at two neighboring points, and gradually increase the number of neighboring points by a linear scheme $2 + \text{data} \times \text{ratio}$ (see the caption of Fig. 13) to test the performances of our method. Fig. 13 shows the mean performances of our method with respect to the different numbers of neighboring points on the seven point sets. Our method generally performs well when the additional number of neighboring points to data ratio is set to 0.012.

According to this result, we chose 23 ($[2 + 1715 * 0.012]$) as a optimized K for Bird2. The performances of the four methods on this point set are given in Fig. 14(a), and the comparison results between $K=5$ and $K=23$ are shown in Fig. 14(b). Registration examples are demonstrated in Fig. 14(c). Based on these results, our method with the initial $K=5$ still gives very accurate results and the best alignments over all degrees of deformation. Furthermore,

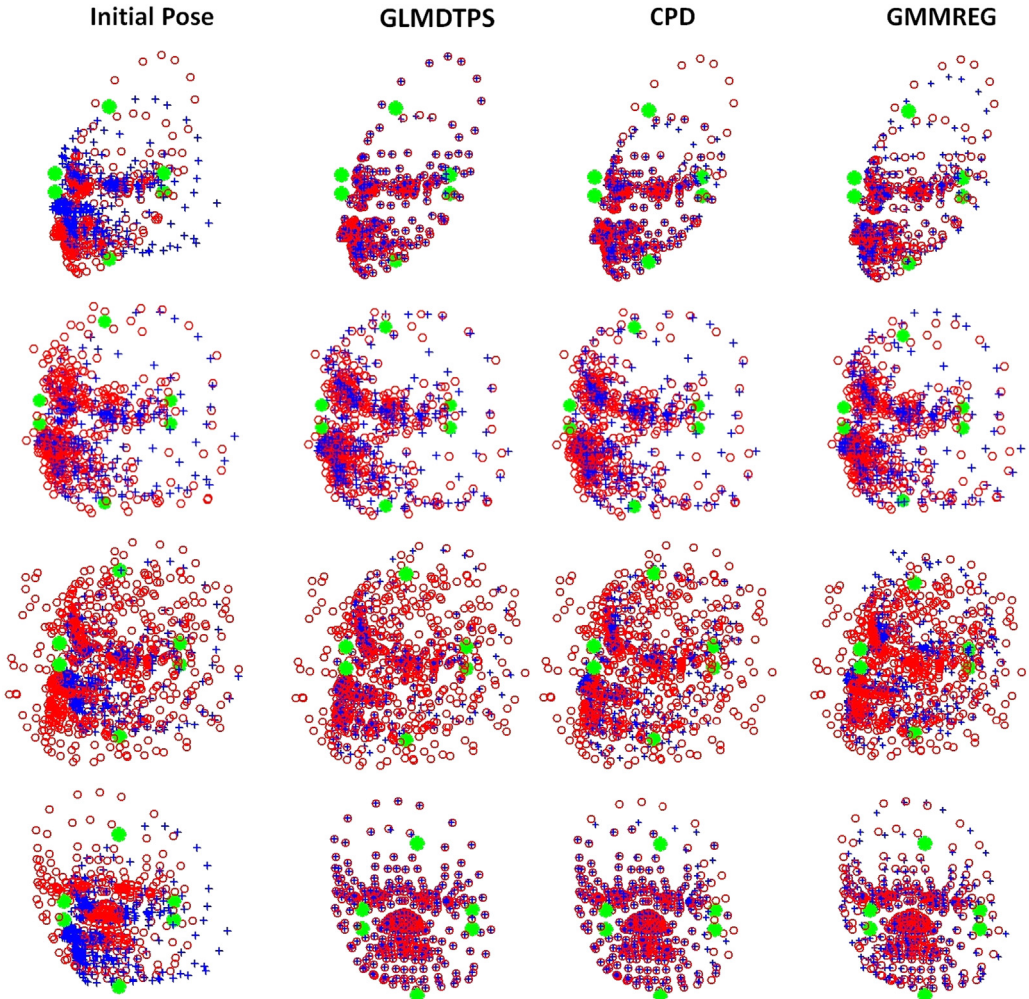


Fig. 8. Registration examples on Face3D. From the top row to bottom row are examples in the deformation (the 4th degree), noise (0.03), outlier (0.8) and rotation (30°) experiments. The green points are the control points for generating deformations. (For interpretation of the references to color in this figure caption, the reader is referred to the web version of this article.)

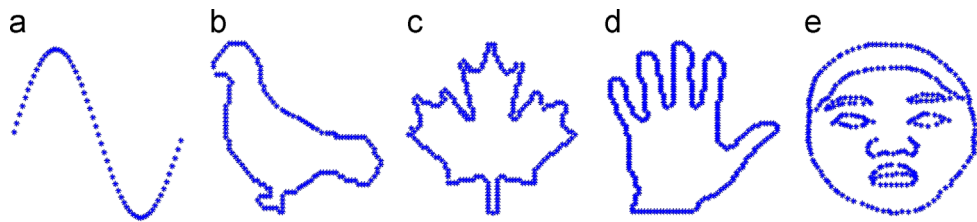


Fig. 9. Additional point sets: (a) Line (60 points) [15], (b) Bird1 (146 points), (c) Maple (215 points), (d) Hand (302 points) and (e) Face2D (317 points).

the accuracy and stability of the performance are obviously improved by using the optimized $K=23$.

Noise, outlier and rotation: Noise is generated by a Gaussian white noise function from the original points such that the points deviate from their original locations and the geometrical shapes represented by the deviated points become fuzzy. The registration process in dealing with noise is similar to the fitting of a set of data points with linear least squares. In our method, minimizing the global distance may be considered to be a linear least squares solution. Therefore, decreasing the number of neighboring points may reduce the influence of minimizing local distances and tend to minimize the global distance more quickly (i.e., minimizing the global distance using more iterations) since the summed local distance has become smaller before reducing α . Moreover, the

outliers in non-rigid point set registration problems are considered as points that markedly deviate from the original points. The outliers disrupt the local structures of the original points. Therefore, using a relatively small number of neighboring points may help to distinguish such outliers since an outlier combined with its fewer neighboring points may not construct a meaningful local structure. In addition, reasonably increasing the number of neighboring points may reduce the influence of rotation since a point combined with more neighboring points may construct a bigger local segment.

To demonstrate the performances of our method with optimized K in noise, outlier and rotation experiments, we chose the Chinese Character (where our method performed relatively poorly in the noise and outlier experiments) and the Face3D for the noise and

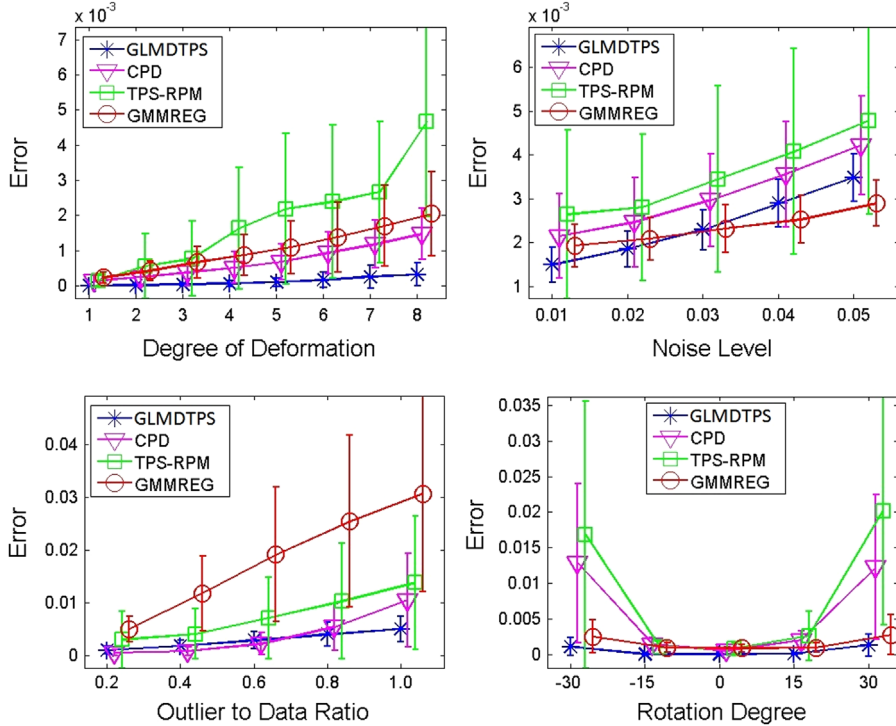


Fig. 10. Mean performances of the four methods on the seven point sets.

Table 3

Scored non-rigid registration results and mean scores on the seven point sets. The D, N, O and R indicate the deformation, noise, outlier and rotation experiments, respectively. The maximum and minimum of summed scores on the seven point sets for each setting are 28 and 7, respectively. If two methods have the same mean error, the two methods will be scored with the same score, and the next rank will be stripped. From left to right, the scores indicate the performances from the first to the eighth degree in the deformation experiments, from 0.01 to 0.05 in the noise experiments, from 0.2 to 1 in the outlier experiments and from -30° to 30° in the rotation experiments.

Methods	D	N	O	R
GLMDTPS	28-28-28-28-28-28-28(28.0)	25-25-25-21-21(23.4)	21-19-22-23-24(21.8)	27-28-28-28-27(27.6)
CPD	18-19-20-20-20-20-20(19.6)	15-14-14-14-14(14.2)	26-28-25-23-21(24.6)	11-10-20-11-13(13.0)
TPS-RPM	15-14-12-10-10-9-9(11.1)	11-11-11-10-9(10.4)	15-16-16-17-18(16.4)	10-17-12-17-12(13.6)
GMMREG	9-9-10-12-12-13-13(11.3)	19-20-20-25-26(22.0)	8-7-7-7-7(7.2)	22-15-10-14-18(15.8)

outlier experiments, and the Fish1 for the rotation experiment. The results are shown in Fig. 15. All the performances are improved by adjusting the number of neighboring points K . Based on these results, the number of neighboring points K combines a more flexible control in dealing with deformation, noise, outliers and rotation with accurate performance.

3.2. Experiments on sequence images

In the second series of experiments, we evaluate the performance of our method in sequence images. Compared with the contour point sets, feature point sets in sequence images have relatively fewer points that sparsely distribute on images. The CMU house is one of the most popular point sets and has been commonly used to test the performances of graph based methods. The house dataset consist of 111 frames and each frame has 30 labeled landmarks. We compared the performance of our method against three state-of-the-art graph based methods: Caetano et al. [9,10], Leordeanu et al. [12] and FGM [11] under all possible image pairs. The results are shown in Table 4. Our method gives the perfect matching results in all possible image pairs, and

outperforms the three graph based methods. One representative matching example is shown in Fig. 16.

3.3. Experiments on real images

In the third series of experiments, we test the performance of our method in the dataset from [12]. This dataset consists of 30 pairs of car images and 20 pairs of motorbike images selected from Pascal 2007 Challenge. Each pair contains 30–60 feature points. We compared the performances of our method against the FGM [11] and Leordeanu et al. [12]. The results are listed in Table 5. Our matching rate is higher than their published results. Matching examples are shown in Fig. 17.

3.4. Computational complexity

The computational cost in our method is mainly related to two aspects: (a) the annealing parameters T_{init} , T_{final} and r which determine the convergence range and (b) the linear assignment solution which determines the worst-cost time of solving the correspondence matrix.

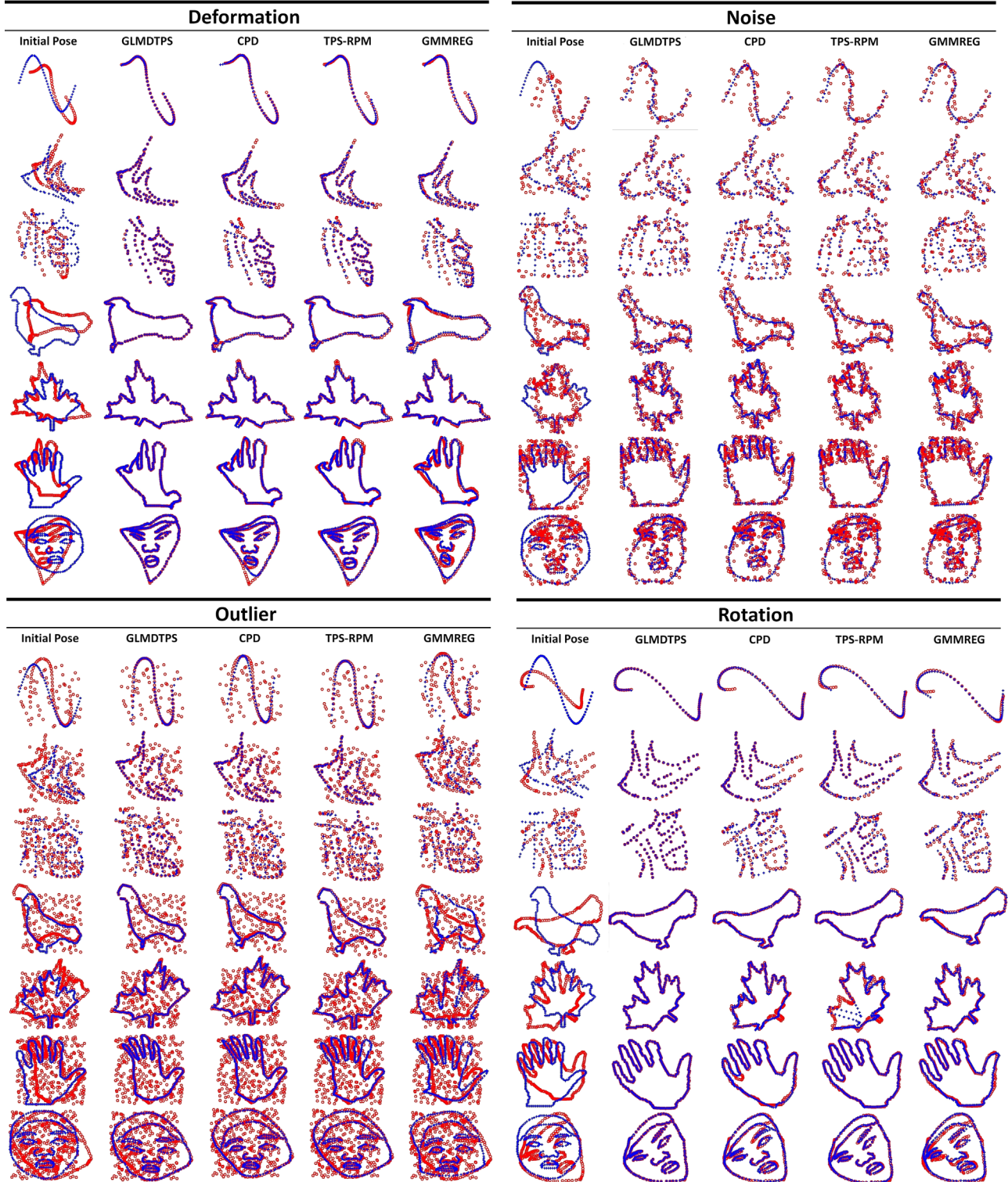


Fig. 11. Registration examples on the seven point sets. All results shown here are under the settings of the 8th degree of deformation, the 3rd noise level, the outlier to data ratio as 1 and the 30° rotation for the deformation, noise, outlier and rotation experiments, respectively. For the noise, outlier and rotation cases, the target point sets were also warped by the 4th degree of deformation.

3.4.1. Convergence range

The convergence range of our method is determined by the deformation degree of target point set since r is fixed as 0.7, and T_{init} and T_{final} are determined by the squared distance between points (see Section 2.4 Annealing parameter setting). In the other three methods, the convergence ranges are determined by the

annealing scheme in the TPS-RPM, and the tolerance stopping criterion and the maximum iteration in the CPD and GMMREG. We investigate the convergence ranges of the four methods under the largest deformation of Fish 1. The parameter settings for the three methods follow the values used in the former Fish 1 experiment. On average, CPD required 33 iterations and TPS-RPM 94 iterations.

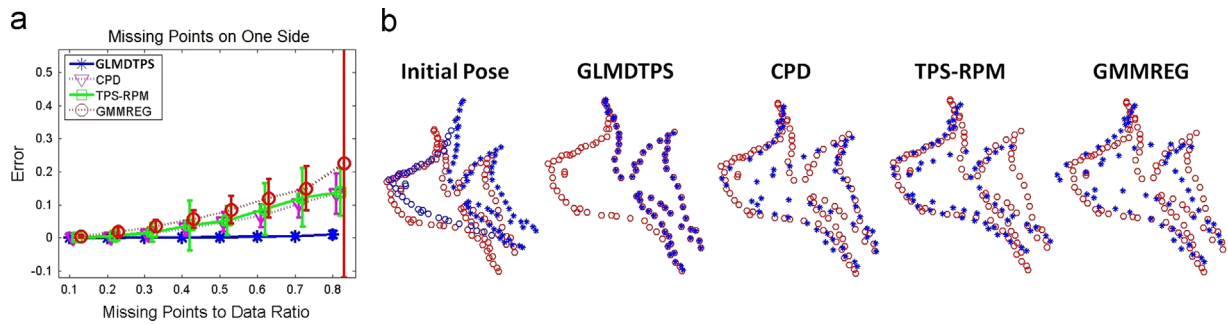


Fig. 12. Performance on partial matching. (a) The parameter settings of our method, TPS-RPM and GMMREG were set as in Fish1 experiment. For CPD, we followed its published setting ($\lambda = 2$, $\beta = 2$ and $w = 0.5$) for the non-rigid missing point case in [23]. (b) Missing points to data ratio: 0.4. The blue circles in the initial pose indicate the missing parts. (For interpretation of the references to color in this figure caption, the reader is referred to the web version of this article.)

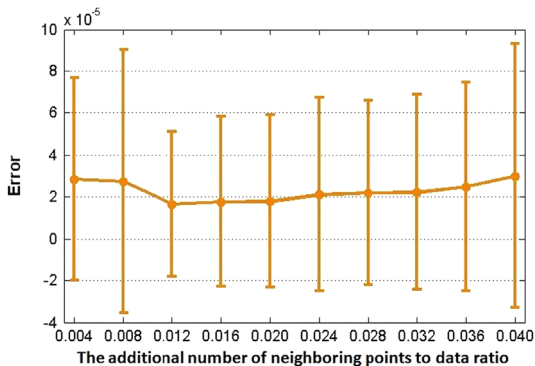


Fig. 13. Mean performances with respect to the different numbers of neighboring points. The x-axis indicates the additional number of neighboring points to data (the number of points in each point set) ratio. The actual number of neighboring points used is equal to 2+data \times ratio.

GMMREG used the maximum number of iterations (100) in all experiments since the stopping criterion of 10^{-10} specified in the original work was unattainable, given that the minimum error numerically attainable during optimization is the square root of the machine precision used to represent the cost [42]. Based on the initial parameter setting (Section 2.4), our method required fewer iterations (an average of 21). To demonstrate the convergences of our method in deformation, noise, outlier and rotation experiments, Fig. 18 shows the registration performances with different iterations on the Fish1 point sets.

In addition, we also investigated the performances of our method with different annealing parameter settings. Fig. 19 shows an example on the Fish1 point set. For each annealing parameter setting, one hundred random experiments were repeated on each deformation degree. According to the results shown in Fig. 19, the performance with reducing the T_{init} was slightly improved and the registration iterations were reduced about 33% (from 21 iterations on average to 14 iterations); the performances with increasing the T_{final} were degraded and the registration iterations were reduced about 33% (from 21 to 14); the performances with reducing the annealing rate r were slightly degraded and the registration iterations were reduced about 62% (from 21 to 8). All the experiments still show very high accuracies (i.e., the errors were less than 0.00023 and the standard deviations were within ± 0.00027) even if the annealing parameters were significantly changed. Based on these results, the computational cost in our method can be substantially reduced by adjusting the annealing parameter settings while still maintaining accurate alignment.

3.4.2. Performance of Jonker–Volgenant algorithm

To solve the correspondence matrix by using a linear assignment solution, the Jonker–Volgenant algorithm [27] which has the worst-cost time $O(N^3)$ has been employed in this work. The time costs on the different sizes of cost matrices are listed in Table 6. The Jonker–Volgenant algorithm demonstrates fast solutions that make our method achieve a fast solution for non-rigid point set registration problems.

3.4.3. Total computational time

In addition to the aforementioned convergence range and linear assignment solution, the total computational time of each method also highly depends on programming languages (e.g., Matlab vs. C++) and code optimization (e.g., using parallel computing and existing optimization tools, and improving memory management). Furthermore, a tradeoff between the computational time and registration accuracy exists and must be adequately considered. Since TPS-RPM is implemented in Matlab and takes a relatively long computational time (about 5.3 s for 100 points and 582 s for 1700 points), we provide an example of computational time vs. number of points only for CPD, GMMREG and our method in Fig. 20(a) and their registration accuracies in Fig. 20(b). Note that CPD is mostly implemented in C++. For GMMREG, the core functions are implemented in C++ and optimization tools are used for the Matlab portions. In our method, only the Jonker–Volgenant algorithm is implemented in C++ while the other parts are implemented in Matlab. GMMREG generally gives the fastest solution. Our method has a very similar computational speed with CPD below 1000 points, and matches (or even surpasses) GMMREG below 400 points. The three methods give different registration accuracies, with our method providing more stable and accurate registration results.

4. Conclusion

We have introduced a global and local mixture distance based non-rigid point set registration method. The method first defined a global distance and a local distance for measuring the global and local structural differences between two point sets, respectively. We then combined the two distances to be a mixture distance based cost matrix to estimate correspondences. An annealing scheme was designed to smoothly control the correspondence estimation and the transformation updating. Carefully designed experiments on contour registration, sequence images and real images were undertaken to demonstrate the robustness and stability of our method. Comparing the performances of our method against the six state-of-the-art methods, our method

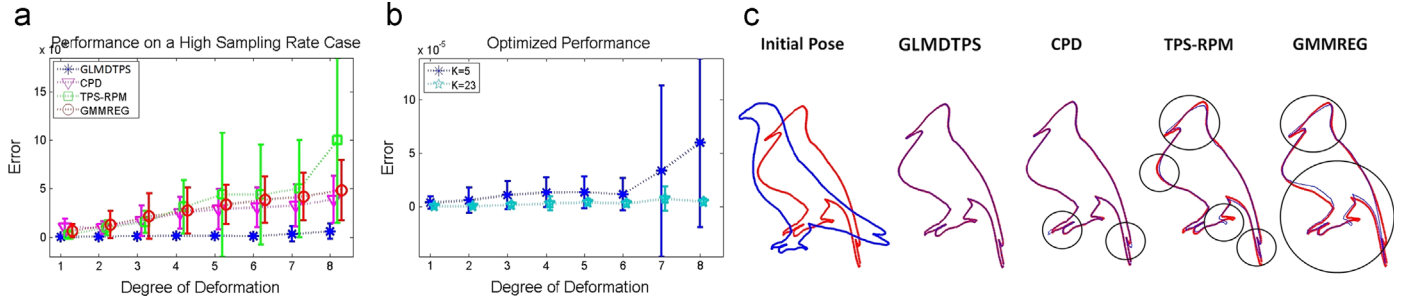


Fig. 14. Performance on high sampling rate case. (a) The performances of the four methods. (b) The performances of our method by using different numbers of neighboring points. (c) Registration examples in the high sampling experiment. The deformation was under the 6th degree. The blue and red shapes indicate the source and target point set, respectively. The parameter settings of the four methods were the same as set in the Fish1 experiment. The mismatches are pointed out by the black circles. (For interpretation of the references to color in this figure caption, the reader is referred to the web version of this article.)

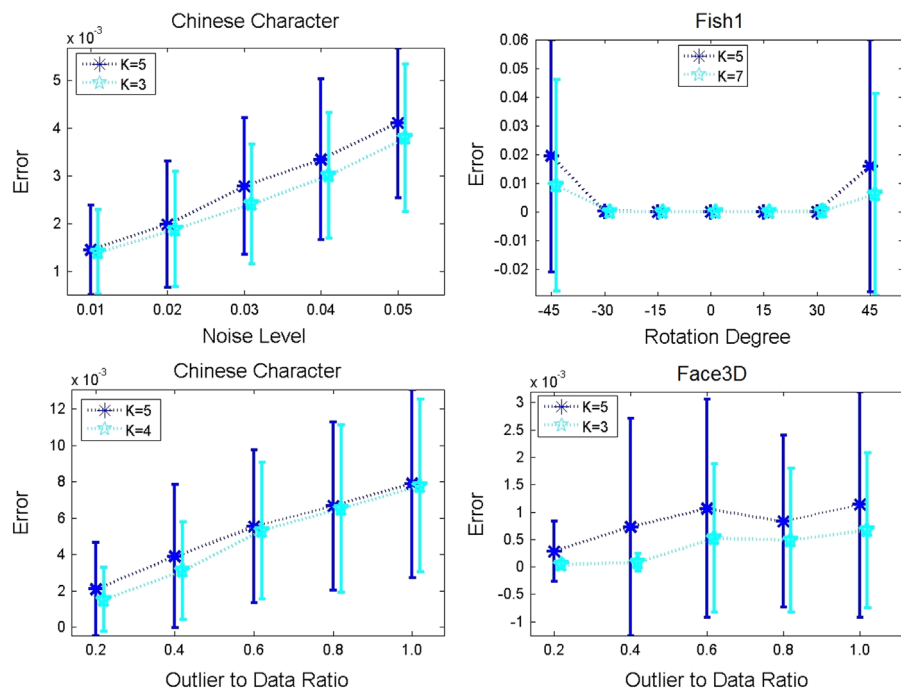


Fig. 15. Performances with optimized K in the noise, outlier and rotation experiments.

Table 4

Matching rates on the CMU house for all possible image pairs. For FGM and Caetano et al. [9], we report upper bounds of their published results. For Leordeanu et al. we report their published results. S and U denote ‘supervised’ and ‘unsupervised’, respectively. The numbers in S and U denote the number of training image pairs.

GLMDTPS $K=5$	FGM	Leordeanu et al.	Caetano et al. $S(106)$	
			$S(5)$	$U(5)$
100%	$\approx 100\%$	99.8%	99.8%	< 96%

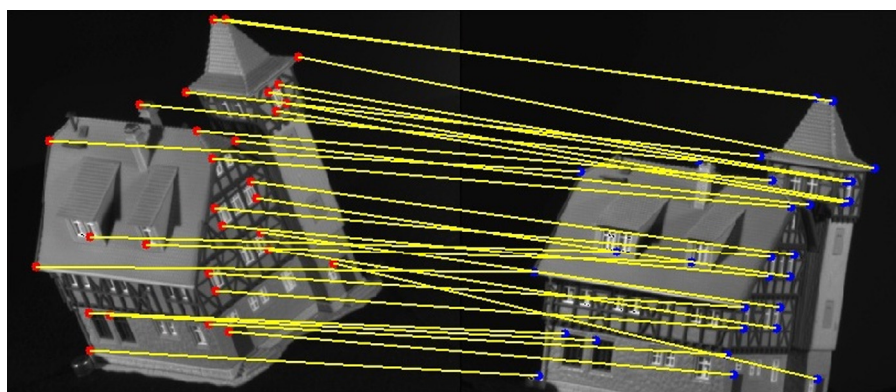


Fig. 16. Wide baseline matching example on the CMU House: the 1st image matching with the 111th image (30/30 correct matches).

shows the best performances in most scenarios. The significant contributions of our work include the following:

- Minimizing the local distance preserves the topological structure of the point sets. Moreover, the Euclidean distance between two point sets is always minimized by the global distance minimization at the end of registration.
- The designed GLMD based cost matrix provides a flexible way to estimate the correspondences between multiple features.

- Unlike the single feature based correspondence estimation in the current methods, the designed annealing scheme combined with the GLMD based cost matrix improves the flexibility and accuracy of the correspondence estimation by using both local and global distance features. Moreover, it also enhances the interaction between the two steps during registration.
- The number of neighboring points K combines greater flexibility in dealing with deformation, noise, outliers and rotation with accurate performance.

Table 5

Matching rates on cars and motorbikes. For the FGM and Leordeanu et al., we report their published results. L: after learning.

GLMDTPS $K=5$	FGM	Leordeanu et al. L
93%	80%	80%

In addition, the idea of building the GLMD based cost matrix creates a new framework ‘Global feature + $\alpha \times$ Local feature’ that allows the employment of multi-feature correspondence estimation. This new framework may lead to more multi-feature based non-rigid point set registration methods in future. We provide the Matlab code of the proposed GLMD algorithm free for academic research.

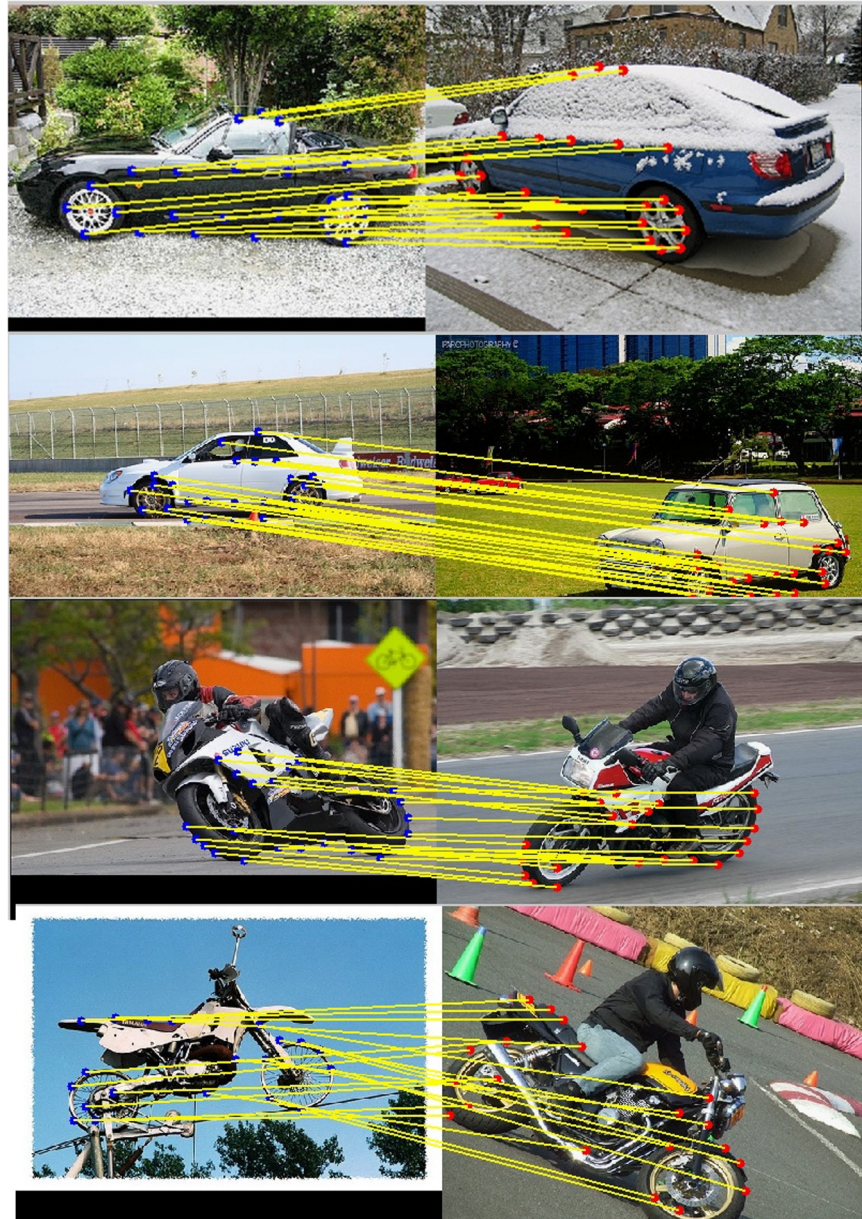


Fig. 17. Matching examples on cars and motorbikes.

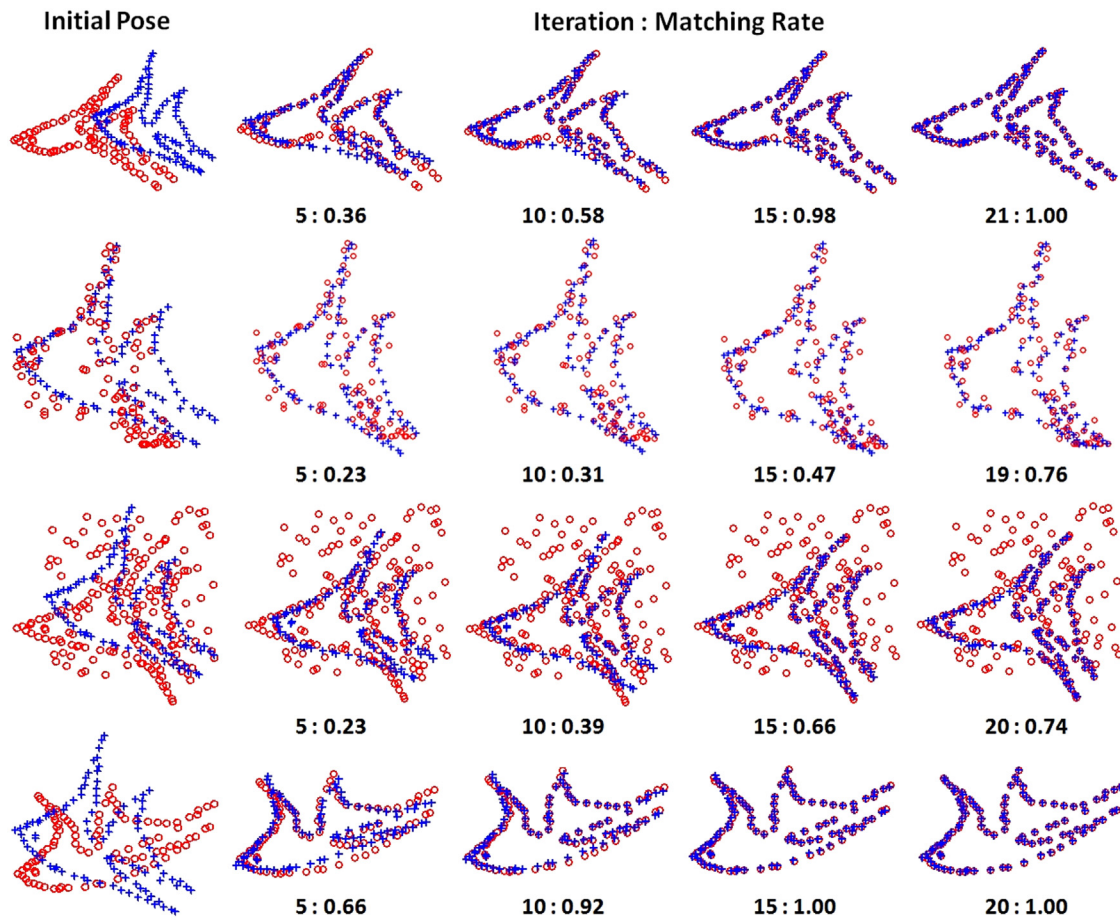


Fig. 18. Registration performances with different iterations. The target point sets (from top to bottom) for deformation, noise, outlier and rotation experiments are set by the 8th degree of deformation, the 3rd noise level, the outlier to data ratio as 1 and the 30° rotation, respectively. For the noise, outlier and rotation, the target point sets were also warped by the 4th degree of deformation.

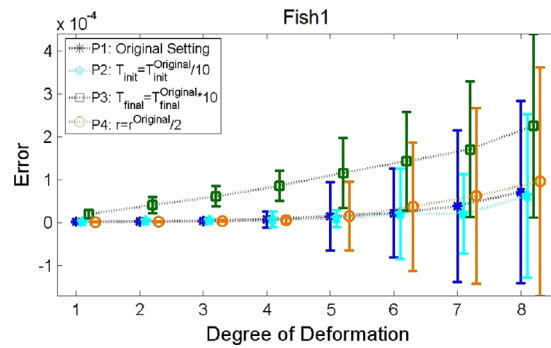


Fig. 19. Relationships between performances and different annealing parameter settings.

Table 6

Performance of Jonker–Volgenant algorithm. We tested the performance of Jonker–Volgenant algorithm in Matlab (using a Mex file) on a PC with 4 GB of RAM and 2.67 GHz Intel(R) Xeon(R) CPU. The cost matrices were generated by Matlab *rand* function.

Size	200	500	1000	2000	3000
Time Cost (s)	0.002	0.016	0.100	0.316	0.588

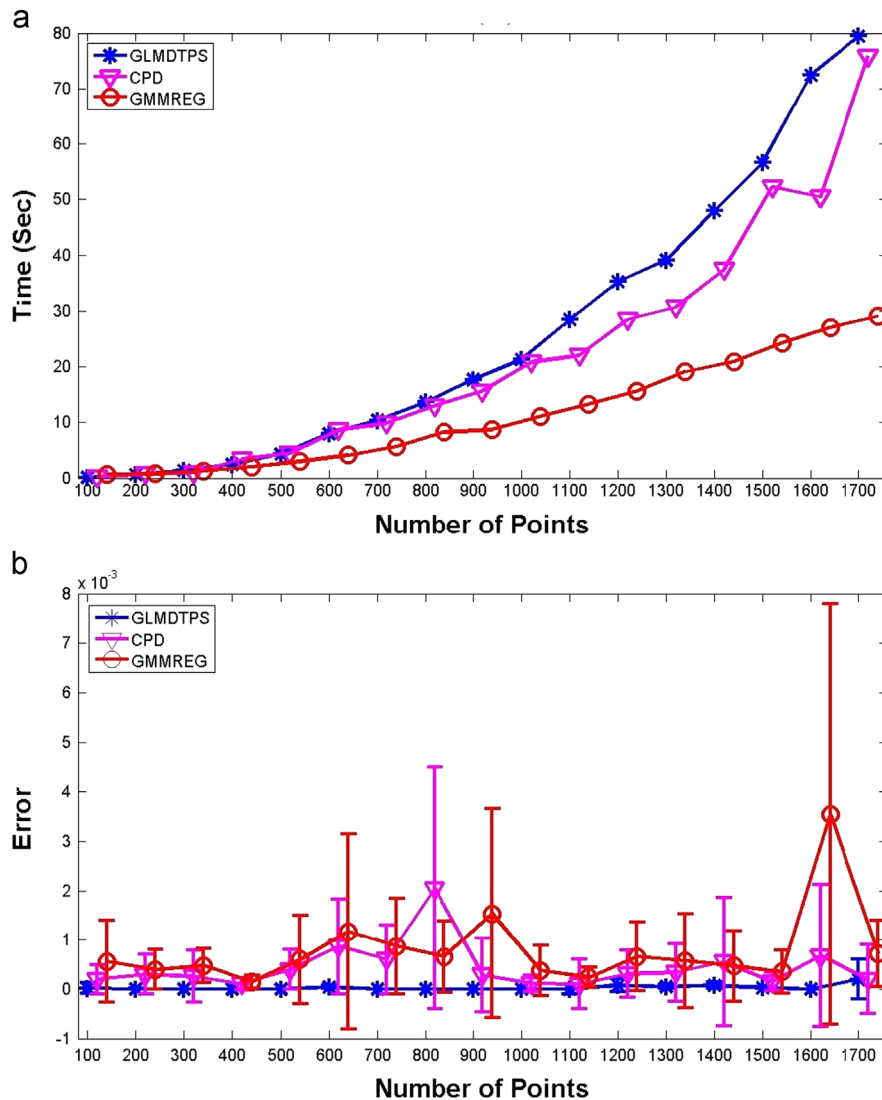


Fig. 20. Example of computational time vs. number of points and registration accuracy. (a) Computational time vs. number of points. (b) Registration accuracy. Bird2 point set (1715 points, used in high sampling rate case of Section 3.1.4) is selected to demonstrate this experiment. We further downsampled Bird2 point set by 100 to 1715 with an interval of 100 points. The results are tested under the largest degree of a random deformation in Matlab (on the same PC used in Table 6). The parameter settings of the three methods followed the same setting in the Fish1 experiment of Section 3.1.1.

Conflict of interest

The authors declare that they have no conflicts of interest in the research.

Acknowledgments

The authors wish to thank Haili Chui, Anand Rangarajan, Andriy Myronenko, Xubo Song, Bing Jian, Baba C. Vemuri, Feng Zhou, Marius Leordeanu and Tiberio S. Caetano for providing their implementation source codes and test datasets. This greatly facilitated the comparison experiments. The support of this research by SBIC Collaborative Grant (RP C-007/2006) is gratefully acknowledged.

References

- [1] S. Park, K. Lee, A line feature matching technique based on an Eigenvector approach, *Comput. Vis. Image Underst.* 77 (2000) 263–283.
- [2] W. Kong, B. Kimia, On solving 2D and 3D puzzles using curve matching, in: Proceedings of the IEEE CS Conference on Computer Vision and Pattern Recognition, vol. 2, 2001, pp. 583–590.
- [3] S. Cochran, G. Medioni, 3D surface description from binocular stereo, *IEEE Trans. Pattern Anal. Mach. Intell.* 14 (1992) 981–994.
- [4] S. Belongie, J. Malik, J. Puzicha, Shape matching and object recognition using shape contexts, *IEEE Trans. Pattern Anal. Mach. Intell.* 24 (2002) 509–521.
- [5] M. Kortgen, G. Park, M. Novotni, R. Klein, 3D shape matching with 3D shape context, in: Proceedings of the 7th Central European Seminar on Computer Graphics, 2003, pp. 22–24.
- [6] V. Balakrishnan, *Graph Theory*, 1st ed., McGraw-Hill, New York, 1997.
- [7] H. Sundar, D. Silver, N. Gagvani, S. Dickinson, Skeleton based shape matching and retrieval, in: Proceedings of the Shape Modeling International (SMI'03), 2003, pp. 130–139.
- [8] Y. Zheng, D. Doermann, Robust point matching for nonrigid shapes by preserving local neighborhood structures, *IEEE Trans. Pattern Anal. Mach. Intell.* 28 (2006) 643–649.
- [9] T. Caetano, L. Cheng, Q. Le, A. Smola, Learning graph matching, in: IEEE 11th International Conference on Computer Vision, 2007, pp. 1–8.
- [10] T. Caetano, J. McAuley, L. Cheng, Q. Le, A. Smola, Learning graph matching, *IEEE Trans. Pattern Anal. Mach. Intell.* 31 (2009) 1048–1058.
- [11] F. Zhou, F. De la Torre, Factorized graph matching, in: IEEE Conference on Computer Vision and Pattern Recognition, 2012, pp. 127–134.
- [12] M. Leordeanu, R. Sukthankar, M. Hebert, Unsupervised learning for graph matching, *Int. J. Comput. Vis.* 96 (2012) 28–45.
- [13] D. Xiao, D. Zahra, P. Bourgeat, P. Berghofer, O. Tamayo, C. Wimberley, M. Gregoire, O. Salvado, An improved 3D shape context based non-rigid registration method and its application to small animal skeletons registration, *Comput. Med. Imaging Graph.* 34 (2010) 321–332.

- [14] B. Jian, B. Vemuri, Robust point set registration using Gaussian mixture models, *IEEE Trans. Pattern Anal. Mach. Intell.* 33 (2011) 1633–1645.
- [15] H. Chui, A. Rangarajan, A new point-matching algorithm for non-rigid registration, *Comput. Vis. Image Underst.* 89 (2003) 114–141.
- [16] A. Rangarajan, H. Chui, F. Bookstein, The softassign Procrustes matching algorithm, in: Information Processing in Medical Imaging (IPMI'97), 1997, pp. 29–42.
- [17] H. Chui, J. Rambo, R. Duncan, A. Rangarajan, Registration of cortical anatomical structures via robust 3D point matching, in: Information Processing in Medical Imaging (IPMI'99), 1999, pp. 168–181.
- [18] S. Gold, A. Rangarajan, C. Lu, S. Pappu, E. Mjolsness, New algorithms for 2D and 3D point matching: pose estimation and correspondence, *Pattern Recognit.* 31 (1998) 1019–1031.
- [19] A. Yuille, Generalized deformable models, statistical physics, and matching problems, *Neural Comput.* 2 (1990) 1–24.
- [20] F. Bookstein, Principal warps: thin-plate splines and the decomposition of deformations, *IEEE Trans. Pattern Anal. Machine Intell.* 11 (1989) 567–585.
- [21] A. Myronenko, X. Song, M. Carreira-Perpinan, Nonrigid point set registration: coherent point drift, *Adv. Neural Inf. Process. Syst.* (2006) 1009–1016.
- [22] A. Yuille, N. Grzywacz, A mathematical analysis of the motion coherence theory, *Int. J. Comput. Vis.* 3 (1989) 155–175.
- [23] A. Myronenko, X. Song, Point set registration: coherent point drift, *IEEE Trans. Pattern Anal. Mach. Intell.* 32 (2010) 2262–2275.
- [24] L. Greengard, J. Strain, The fast Gauss transform, *J. Sci. Stat. Comput.* 12 (1991) 79–94.
- [25] I. Markovsky, Structured low-rank approximation and its applications, *Automatica* 44 (2008) 891–909.
- [26] L. Ruschendorf, S. Rachev, A characterization of random variables with minimum L2 distance, *J. Multivar. Anal.* 32 (1990) 48–54.
- [27] R. Jonker, A. Volgenant, A shortest augmenting path algorithm for dense and sparse linear assignment problems, *Computing* 38 (1987) 325–340.
- [28] M. Miller, H. Stone, I. Cox, Optimizing Murty's ranked assignment method, *IEEE Trans. Aerosp. Electron. Syst.* 33 (1997) 851–862.
- [29] G. Wahba, Spline Models for Observational Data, SIAM, Philadelphia, 1990.
- [30] R. Durbin, R. Szekli, A. Yuille, An analysis of the elastic net approach to the traveling salesman problem, *Neural Comput.* 1 (1989) 348–358.
- [31] P. Mahalanobis, On the generalised distance in statistics, *Proc. Indian Natl. Sci. Acad. Phys. Sci.* 2 (1936) 49–55.
- [32] TPS-RPM, This is the URL of TPS-RPM source codes, 2003. URL: <http://noodle.med.yale.edu/chui/tps-rpm.html>.
- [33] CPD, This is the URL of CPD source codes, 2010. URL: <https://sites.google.com/site/myronenko/research/cpd>.
- [34] GMMREG, This is the URL of GMMREG source codes, 2011. URL: <https://code.google.com/p/gmmreg/>.
- [35] Y. Yang, K. Foong, S. Ong, M. Yagi, K. Takada, A new methodology for studying the functional activity of lateral pterygoid muscle, in: 62nd American Academy of Oral and Maxillofacial Radiology Annual Meeting, 2011, p. 67.
- [36] Y. Yang, K. Foong, S. Ong, M. Yagi, K. Takada, An image-based method for quantification of masseter muscle deformation, in: The 5th International Conference on Biomedical Engineering and Informatics, 2012, pp. 190–194.
- [37] Y. Yang, K. Foong, S. Ong, M. Yagi, K. Takada, Image-based estimation of biomechanical relationship between masticatory muscle activities and mandibular movement, in: The IEEE 12th International Conference on Bioinformatics and Bioengineering, 2012, pp. 683–688.
- [38] Y. Yang, K. Foong, S. Ong, M. Yagi, K. Takada, An image-based method for quantification of lateral pterygoid muscle deformation, in: The IEEE 12th International Conference on Bioinformatics and Bioengineering, 2012, pp. 698–702.
- [39] D. Liao, J. Zhao, H. Gregersen, A novel 3D shape context method based strain analysis on a rat stomach model, *J. Biomech.* 45 (2012) 1566–1573.
- [40] M. Urschler, H. Bischof, Assessing breathing motion by shape matching of lung and diaphragm surfaces, in: Proceedings of SPIE Conference on Medical Imaging: Physiology, Function, and Structure from Medical Images, vol. 5746, 2005, pp. 440–452.
- [41] O. Acosta, J. Fripp, V. Dore, P. Bourgeat, J. Favreau, G. Chetelat, A. Rueda, V. Villemagne, C. Szeke, D. Ames, K. Ellis, R. Martins, C. Masters, C. Rowe, E. Bonner, F. Gris, D. Xiao, P. Raniga, V. Barra, O. Salvador, Cortical surface mapping using topology correction, partial flattening and 3D shape context-based non-rigid registration for use in quantifying atrophy in Alzheimer's disease, *J. Neurosci. Methods* 205 (2012) 96–109.
- [42] W. Press, S. Teukolsky, W. Vetterling, B. Flannery, Numerical Recipes in C: The Art of Scientific Computing, Cambridge University Press, Cambridge, 1992.

Yang Yang received the BS and MS degrees from the Chiba Institute of Technology, Japan and the Waseda University, Japan, in 2004 and 2007, respectively, and worked toward the Ph.D. degree in the NUS Graduate School for Integrative Sciences and Engineering, National University of Singapore from August 2009 to April 2013. He is currently working with the School of Information Science and Technology, Yunnan Normal University, China. His research interests broadly include computer vision, machine learning, medical imaging and geographic information system areas.

Sim Heng Ong received the B.E.(Hons.) degree from the University of Western Australia, Perth, WA, Australia, and the Ph.D. degree from the University of Sydney, Sydney, NSW, Australia. He is currently an Associate Professor in the Department of Electrical Engineering and the Department of Bioengineering, National University of Singapore, Singapore. His current research interests include computer vision and biomedical image processing. He has authored or coauthored more than 250 papers published in international journals and conference proceedings.

Kelvin Weng Chiong Foong is a specialist dental surgeon. He graduated from the National University of Singapore with the Dental degree in 1988, and received speciality training at The University of Adelaide, Australia, from 1992 to 1994, and the Ph.D. degree in 2005, having studied the topic of 3D surface imaging of cleft palate deformity in infants. He is currently an Associate Professor in the Faculty of Dentistry, National University of Singapore. He also holds the appointment of Senior Consultant in Orthodontics at the National University Hospital. His current research interests include the application of 3-D image processing and visualization techniques for the development of accurate, patient-specific virtual models of the teeth, face, and head. He works in close collaboration with research partners in the fields of Vision Engineering and Image Processing to develop virtual models of the face and teeth.